Annals of Nuclear Medicine Vol. 17, No. 6, 427–434, 2003

Spectral analysis: principle and clinical applications

Kenya MURASE

Department of Medical Physics and Engineering, Division of Medical Technology and Science, Course of Health Science, Graduate School of Medicine, Osaka University

This review article describes the principle and clinical applications of spectral analysis. Spectral analysis provides a spectrum of the kinetic components which are involved in the regional uptake and partitioning of tracer from the blood to the tissue. This technique allows the tissue impulse response function to be derived with minimal modeling assumptions. Spectral analysis makes no *a priori* assumptions regarding the number of compartments or components required to describe the time course of tracer in the tissue. Spectral analysis can be applied to various dynamic data acquired by planar scintigraphy, single photon emission computed tomography (SPECT) or positron emission tomography (PET) as an alternative approach to compartment analysis. This analysis appears to be clinically useful, because it not only facilitates the interpretation of dynamic scintigraphic, SPECT or PET data, but also simplifies comparisons between regions and between subjects.

Key words: spectral analysis, principle, clinical applications, compartment analysis, dynamic scintigraphy, SPECT, PET

INTRODUCTION

SPECTRAL ANALYSIS is based on the formulation of a constrained linear optimization problem, and is a development of an approach originally applied by Tobler and Engel[1] to the analysis of data obtained *in vitro*.

Spectral analysis was first introduced by Cunningham and Jones[2] in the field of nuclear medicine as a technique for use with dynamic positron emission tomography (PET) studies. This technique is based on the actual kinetic components which can be identified within a given datum set, rather than being restricted, for example, to a predefined compartment model, and allows for the distinction between transit components associated with tracer in the vasculature, and reversible and irreversible components involved in the tissue without *a prior* assumptions regarding the number of components.[2] This method provides a spectrum of the kinetic components which are involved in the regional uptake and partitioning of tracer from the blood to the tissue.[2] This technique allows the tissue impulse response function to be derived with minimal modeling assumptions.[2]

In this review, we describe the principle and clinical applications of spectral analysis, based on our experience.

PRINCIPLE OF SPECTRAL ANALYSIS

In spectral analysis, the radioactivity in the tissue at a given time t [$C(t)$] is modeled as a convolution of the blood input function [$C_a(t)$] with a sum of k exponential terms as

$$C(t) = \sum_{i=1}^{k} \alpha_i \cdot \int_0^t C_a(\tau) e^{-\beta_i (t-\tau)} d\tau, \qquad (1)$$

where α_i and β_i ($\beta_1 < \beta_2 < \ldots < \beta_k$) are assumed to be positive or zero. The upper limit, k, represents the maximum number of terms to be included in the model and this is set to a large number. When $C_a(t)$ is replaced by Dirac's delta function in equation (1), the tissue impulse response function [IRF(t)] can be given by

$$\mathrm{IRF}(t) = \sum_{i=1}^{k} \alpha_i \cdot e^{-\beta_i t}. \qquad (2)$$

Received June 19, 2003, revision accepted June 19, 2003.

For reprint contact: Kenya Murase, Dr. Med. Sci., Dr. Eng., Department of Medical Physics and Engineering, Division of Medical Technology and Science, Course of Health Science, Graduate School of Medicine, Osaka University, 1–7 Yamadaoka, Suita, Osaka 565–0871, JAPAN.

E-mail: murase@sahs.med.osaka-u.ac.jp

Calculation of spectrum

When the β values are given beforehand, the convolution integrals in equation (1) can be calculated using the measured $C_a(t)$. Then, the discrete form of equation (1) can be expressed by the following linear algebraic equation:

$$\begin{cases} C(t_1) = \alpha_1 \cdot f_1(\beta_1) + \alpha_2 \cdot f_1(\beta_2) + \cdots + \alpha_k \cdot f_1(\beta_k) \\ C(t_2) = \alpha_1 \cdot f_2(\beta_1) + \alpha_2 \cdot f_2(\beta_2) + \cdots + \alpha_k \cdot f_2(\beta_k) \\ \quad \vdots \qquad\quad \vdots \qquad\quad \vdots \qquad\quad \cdots \qquad\quad \vdots \\ C(t_m) = \alpha_1 \cdot f_m(\beta_1) + \alpha_2 \cdot f_m(\beta_2) + \cdots + \alpha_k \cdot f_m(\beta_k) \end{cases}, \quad (3)$$

where m denotes the time index and $f_i(\beta_j)$ is given by

$$f_i(\beta_j) = \int_0^{t_i} C_a(\tau) e^{-\beta_j(t_i - \tau)} d\tau. \quad (4)$$

Equation (3) can be given in a matrix form as

$$\vec{C} = \vec{A} \cdot \vec{B}, \quad (5)$$

where

$$\vec{A} = \begin{bmatrix} f_1(\beta_1) & f_1(\beta_2) & \cdots & f_1(\beta_k) \\ f_2(\beta_1) & f_2(\beta_2) & \cdots & f_2(\beta_k) \\ \vdots & \vdots & \cdots & \vdots \\ f_m(\beta_1) & f_m(\beta_2) & \cdots & f_m(\beta_k) \end{bmatrix}, \vec{B} = \begin{bmatrix} \alpha_1 \\ \alpha_2 \\ \vdots \\ \alpha_k \end{bmatrix} \text{ and } \vec{C} = \begin{bmatrix} C(t_1) \\ C(t_2) \\ \vdots \\ C(t_m) \end{bmatrix}.$$

The α value corresponding to each β can be easily obtained from equation (5) using the non-negative least squares method.[3] We call these α values "spectrum" from an analogy of time-frequency analysis.

Relationship between tissue impulse response function and spectrum

In the following, we show the relationship between IRF(t) and the spectrum obtained by spectral analysis for various compartment models.

The first example is a two-compartment model, which is illustrated in Figure 1 (a). In Figure 1 (a), K_1 and k_2 denote the unidirectional clearance rate of tracer from blood to tissue and the rate constant for the transfer of tracer from tissue to blood, respectively. In this case, IRF(t) is given by

$$\text{IRF}(t) = \alpha_1 \cdot e^{-\beta_1 t}, \quad (6)$$

where α_1 and β_1 are equal to K_1 and k_2, respectively. This is illustrated in Figure 1 (b). When using spectral analysis, the spectrum shown in Figure 1 (c) is obtained. In this case, a peak with a height equal to α_1 or K_1 is observed at β equal to β_1 or k_2. When there is no transfer of the tracer from tissue to blood, IRF(t) becomes

$$\text{IRF}(t) = \alpha_1. \quad (7)$$

In this case, the location of the peak in the spectrum moves to β equal to zero.

The second example is a three-compartment model, which is illustrated in Figure 2 (a). In this case, IRF(t) is given by

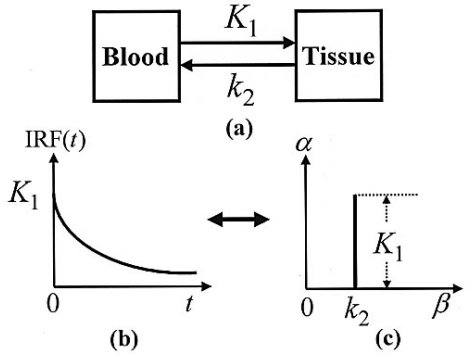

Fig. 1 Illustration of the relationship between the tissue impulse response function and the spectrum obtained by spectral analysis for two-compartment model. Figures 1 (a), 1 (b), and 1 (c) illustrate two-compartment model, the tissue impulse response function, and the spectrum obtained by spectral analysis, respectively.

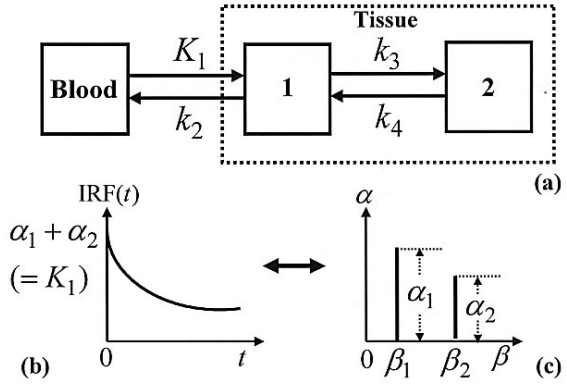

Fig. 2 Illustration of the relationship between the tissue impulse response function and the spectrum obtained by spectral analysis for three-compartment model. Figures 2 (a), 2 (b), and 2 (c) illustrate three-compartment model, the tissue impulse response function, and the spectrum obtained by spectral analysis, respectively.

$$\text{IRF}(t) = \alpha_1 \cdot e^{-\beta_1 t} + \alpha_2 \cdot e^{-\beta_2 t}, \quad (8)$$

which is illustrated in Figure 2 (b). The spectrum is illustrated in Figure 2 (c). As shown in Figure 2 (c), two peaks with heights equal to α_1 and α_2 are observed at β equal to β_1 and β_2, respectively. When there is no transfer of the tracer from compartment 2 to compartment 1, that is, $k_4 = 0$, IRF(t) becomes

$$\text{IRF}(t) = \alpha_1 + \alpha_2 \cdot e^{-\beta_2 t}. \quad (9)$$

In this case, the peak located at $\beta = \beta_1$ moves to $\beta = 0$.

Finally, we consider $(N + 1)$-compartment model as a general case [Fig. 3 (a)]. In this case, IRF(t) is given by

$$\text{IRF}(t) = \alpha_1 \cdot e^{-\beta_1 t} + \alpha_2 \cdot e^{-\beta_2 t} + \cdots + \alpha_N \cdot e^{-\beta_N t}, \quad (10)$$

which is illustrated in Figure 3 (b), and the spectrum shown in Figure 3 (c) is obtained. As shown in Figure 3 (c), N peaks with heights equal to α_1, α_2, . . . and α_N are

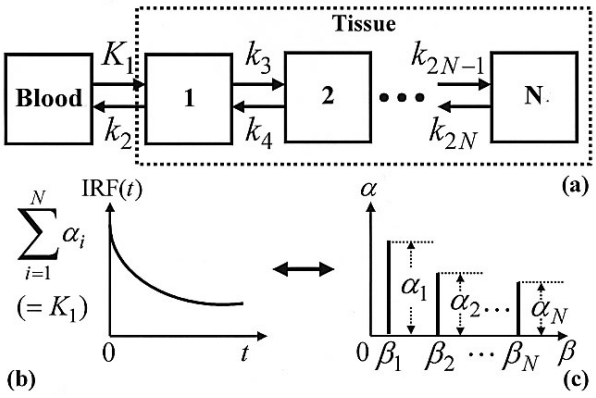

Fig. 3 Illustration of the relationship between the tissue impulse response function and the spectrum obtained by spectral analysis for $(N + 1)$-compartment model. Figures 3 (a), 3 (b), and 3 (c) illustrate $(N + 1)$-compartment model, the tissue impulse response function, and the spectrum obtained by spectral analysis, respectively.

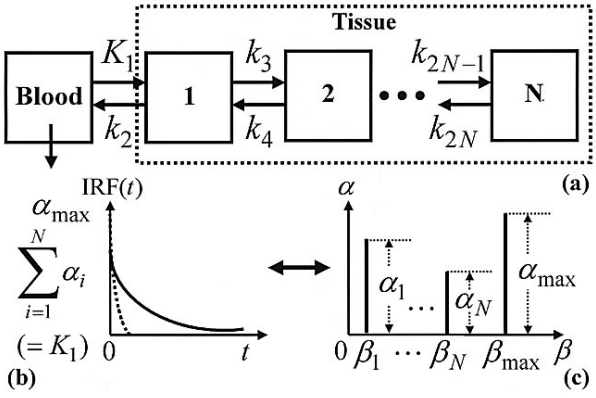

Fig. 4 Illustration of the spectrum obtained by spectral analysis for the $(N + 1)$-compartment model in which there is an intravascular component. Figures 4 (a), 4 (b), and 4 (c) illustrate $(N + 1)$-compartment model, the tissue impulse response function, and the spectrum obtained by spectral analysis, respectively.

observed at β equal to β_1, β_2, . . . and β_N, respectively. When there is no transfer of the tracer from compartment N to compartment N-1, that is, $k_{2N} = 0$, IRF(t) is given by

$$\mathrm{IRF}(t) = \alpha_1 + \alpha_2 \cdot e^{-\beta_2 t} + \cdots + \alpha_N \cdot e^{-\beta_N t}. \quad (11)$$

In this case, the peak located at $\beta = \beta_1$ moves to $\beta = 0$.

When there is an intravascular component in the $(N + 1)$-compartment model, IRF(t) is given by

$$\mathrm{IRF}(t) = \alpha_1 \cdot e^{-\beta_1 t} + \alpha_2 \cdot e^{-\beta_2 t} + \cdots + \alpha_N \cdot e^{-\beta_N t} + \alpha_{\max} \cdot e^{-\beta_{\max} t}. \quad (12)$$

In this case, the spectrum shown in Figure 4 (c) is obtained. As illustrated in Figure 4 (c), another peak usually appears at the largest β.

Derivation of quantitative parameters

When there is no intravascular component, the sum of the heights of the peaks appearing in the spectrum, that is, the α values, is equal to K_1. Therefore, K_1 is given by

$$K_1 = \alpha_1 + \alpha_2 + \cdots + \alpha_k. \quad (13)$$

The mean transit time (MTT) of tracer in the tissue is given by

$$\mathrm{MTT} = \frac{\int_0^\infty \mathrm{IRF}(t)dt}{\mathrm{IRF}(0)}. \quad (14)$$

Substituting equation (2) into equation (14) yields

$$\mathrm{MTT} = \frac{\alpha_1/\beta_1 + \alpha_2/\beta_2 + \cdots + \alpha_k/\beta_k}{\alpha_1 + \alpha_2 + \cdots + \alpha_k}. \quad (15)$$

Computer simulation

We performed computer simulations to validate the quantitative parameters obtained by spectral analysis in comparison with those obtained by compartment analysis.

As an illustrative example, we used the three-compartment fluorodeoxyglucose (FDG) model[4,5] in which the dephosphorylation of FDG-6-phosphate to FDG and the amount of radioactivity attributable to the vascular compartment were assumed to be negligible for the sake of simplicity. This is one of the most popular and established kinetic models. With this model, the amount of radioactivity measured during the ith scan (M_i) can be expressed by

$$M_i = \frac{\int_{T_{i-1}}^{T_i} M(t)dt}{T_i - T_{i-1}}, \quad (16)$$

where T_{i-1} and T_i are the start and end times of the ith scan, respectively, and $M(t)$ is given by[4,5]

$$M(t) = \frac{K_1 \cdot k_3}{k_2 + k_3} \int_0^t C_a(\tau)d\tau + \frac{K_1 \cdot k_2}{k_2 + k_3} \int_0^t C_a(\tau) e^{-(k_2+k_3)(t-\tau)} d\tau. \quad (17)$$

K_1, k_2 and k_3 in the above equation represent the unidirectional clearance of FDG from the blood to the brain, the fractional clearance of FDG from the brain to the blood and the phosphorylation coefficient of FDG to FDG-6-phosphate, respectively, and $C_a(t)$ is the arterial plasma FDG concentration at time t.

'Noiseless' brain time-activity data were generated from a set of K_1, k_2 and k_3, and the plasma time-activity data from PET studies,[6,7] using equation (17). The M_i values given by equation (16) were generated over a set of intervals using the following scanning sequence: six 30-sec, seven 1-min, five 2-min and ten 5-min scans.[6,7]

As previously described, IRF(t) in the 3-compartment model with 3 parameters is given by equation (9). α_1, α_2 and β_2 in equation (9) can be expressed using K_1, k_2 and

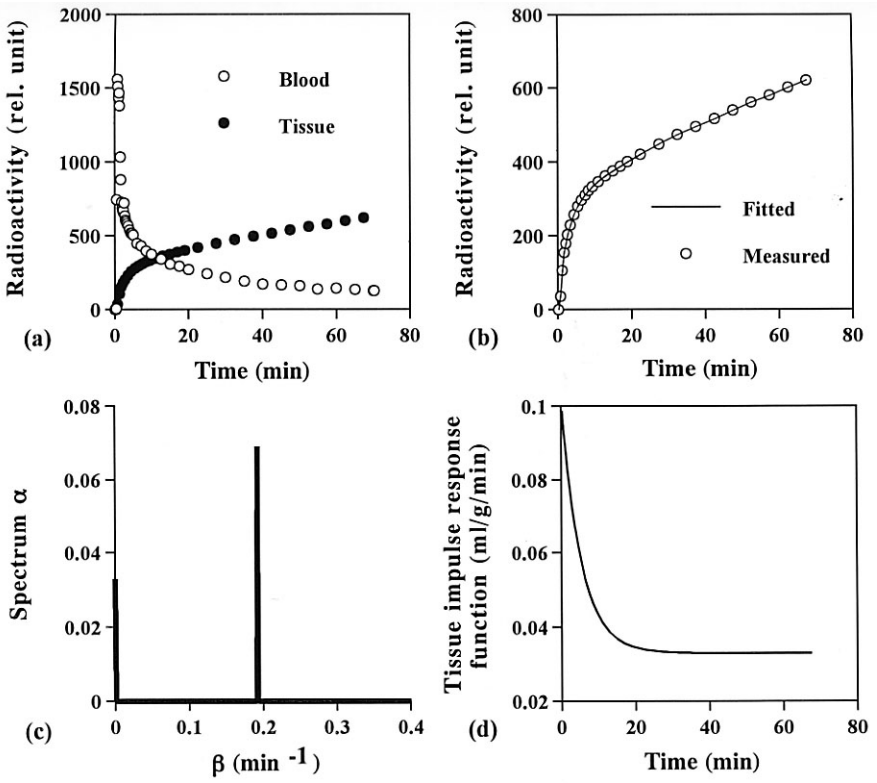

Fig. 5 Example of spectral analysis applied to 3-compartment model with 3 parameters. The open and closed circles in Figure 5 (a) show the time-activity curves of fluorodeoxyglucose (FDG) in the arterial blood and brain tissue, respectively. The open circles and solid line in Figure 5 (b) show the measured time-activity curve in the brain tissue and that estimated from the tissue impulse response function obtained by spectral analysis, respectively. Figure 5 (c) is spectral analysis of tissue response, while Figure 5 (d) is the corresponding tissue impulse response function.

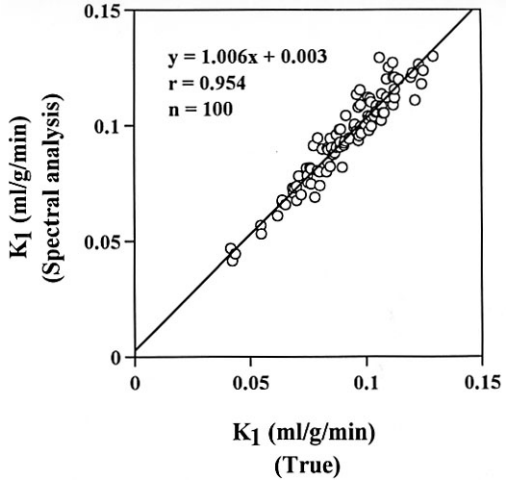

Fig. 6 Relationship between the K_1 values obtained by spectral analysis and the true values.

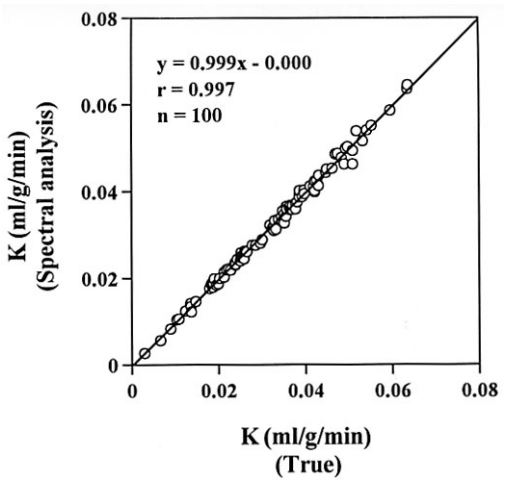

Fig. 7 Relationship between the K values obtained by spectral analysis and the true values.

k_3 by the following equations: $\alpha_1 = K_1 \cdot k_3/(k_2 + k_3) = K$, $\alpha_2 = K_1 \cdot k_2/(k_2 + k_3)$ and $\beta_2 = k_2 + k_3$. Figure 5 shows an example of the results of spectral analysis when applied to this model. Figure 5 (a) shows the time-activity curves of FDG in the arterial blood (*open circles*) and brain tissue (*closed circles*), respectively, while Figure 5 (b) shows the measured time-activity curve in the brain tissue (*open circles*) and that estimated from the tissue impulse re-

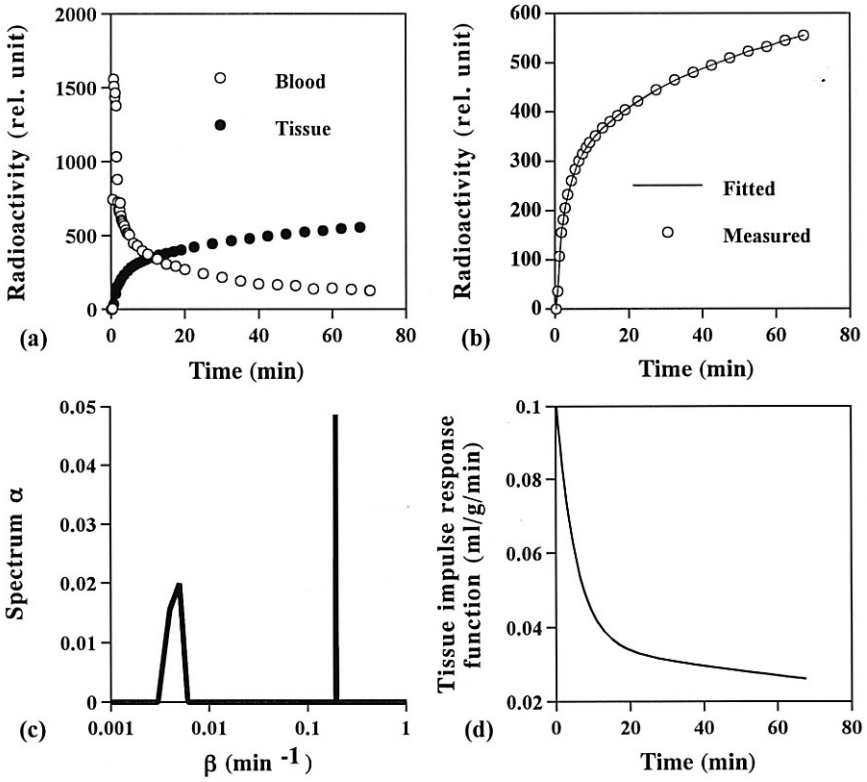

Fig. 8 Example of spectral analysis applied to 3-compartment model with 4 parameters. The open and closed circles in Figure 8 (a) show the time-activity curves of FDG in the arterial blood and brain tissue, respectively. The open circles and solid line in Figure 8 (b) show the measured time-activity curve in the brain tissue and that estimated from the tissue impulse response function obtained by spectral analysis, respectively. Figure 8 (c) is spectral analysis of tissue response, while Figure 8 (d) is the corresponding tissue impulse response function.

sponse function obtained by spectral analysis (*solid line*). Figures 5 (c) and 5 (d) show the spectrum and the tissue impulse response function obtained by spectral analysis, respectively. As expected, there were two peaks in the spectrum, with one peak located at $\beta = 0$ [Fig. 5 (c)]. As previously described, the sum of the heights of the two peaks corresponds to K_1, and the height of the peak located at $\beta = 0$ is equal to α_1, that is, K. Figure 6 shows the relationship between the K_1 values thus obtained by spectral analysis and the true values, while Figure 7 shows the case of the K value. As shown in Figures 6 and 7, there were excellent agreements between the parameters estimated using spectral analysis and the true values, indicating that the quantitative parameters can also be obtained by spectral analysis.

Figure 8 shows a typical result of spectral analysis when applied to 3-compartment model with 4 parameters, in which the dephosphorylation of FDG-6-phosphate to FDG (k_4) exists. It should be noted that there is no peak at $\beta = 0$ in the spectrum [Fig. 8 (c)] unlike the 3-compartment model with 3 parameters [Fig. 5 (c)], and IRF(t) decreases with time [Fig. 8 (d)].

CLINICAL APPLICATION

Spectral analysis can be applied to various dynamic data acquired by planar scintigraphy, single photon emission computed tomography (SPECT) or PET. In the following, we show some clinical applications of spectral analysis using our data.

The first example is the application to hepatobiliary dynamic scintigraphy with ^{99m}Tc-*N*-pyridoxyl-5-methyltryptophan (PMT).[8,9] In this study, we applied spectral analysis to hepatobiliary dynamic scintigraphy with PMT in 82 patients with a wide range of liver function, and compared it with compartment analysis and deconvolution analysis. The rate of uptake of PMT by the liver from the blood (K_1) obtained by spectral analysis (y, min^{-1}) agreed well with the K_1 value obtained using compartment analysis (x, min^{-1}) ($y = 1.079x + 0.000$, r = 0.993, SEE = 0.042 min^{-1}). The mean residence time (MRT) of PMT in the liver obtained by spectral analysis (y, min) also agreed well with the MRT value obtained by deconvolution analysis (x, min) ($y = 1.036x - 0.759$, r = 0.967, SEE = 1.014 min) and that obtained by compartment analysis (x, min) ($y = 0.859x + 1.006$, r = 0.931, SEE

= 1.428 min). The fraction of the measured blood radioactivity superimposed on the true liver radioactivity (f) obtained by spectral analysis (y) correlated well with the f value obtained by compartment analysis (x) ($y = 1.168x - 0.004$, r = 0.924, SEE = 0.043). We conclude that the application of spectral analysis to hepatobiliary dynamic scintigraphy with PMT appears to be useful in evaluating the functional status of the liver, since it facilitates the interpretation of the kinetic parameter of PMT in the liver and allows us to extract quantitative parameters corresponding to those obtained by compartment analysis or deconvolution analysis. Fukui et al.[9] applied this method to assessment of liver function in chronic liver diseases and regional function of irradiated liver, and found that this method helps clarify changes in regional function of the irradiated liver.

The second example is the application to the measurement of the hepatic extraction fraction of hepatobiliary radiopharmaceuticals.[10] Measuring the hepatic extraction fraction (HEF) of a hepatobiliary radiopharmaceutical helps to differentiate hepatocyte diseases from biliary tract ones, and it is generally performed using deconvolution analysis. In this study, we measured HEF using spectral analysis. With spectral analysis, HEF was calculated from (the sum of the spectral data obtained by spectral analysis – the highest frequency component of the spectrum) ÷ (the sum of the spectral data) × 100 (%). We applied this method to dynamic liver scintigraphic data obtained from six healthy volunteers and from 46 patients with various liver diseases, using PMT. We also measured HEF using deconvolution analysis, in which the modified Fourier transform technique was employed. The HEF values obtained by spectral analysis correlated closely with those obtained by deconvolution analysis (r = 0.925), suggesting that our method is valid. The HEF values obtained by spectral analysis decreased as the severity of liver disease progressed. The values were 100 ± 0.0%, 94.7 ± 13.6%, 76.2 ± 27.4%, 45.7 ± 15.6%, 82.7 ± 24.2% and 95.2 ± 11.8% (mean ± SD) for the normal controls (n = 6), mild liver cirrhosis (n = 16), moderate liver cirrhosis (n = 11), severe liver cirrhosis (n = 5), acute hepatitis (n = 8) and chronic hepatitis groups (n = 6), respectively. The HEF was obtained more simply and rapidly by spectral analysis than by deconvolution analysis. The results suggest that our method using spectral analysis can be used as an alternative to the conventional procedure using deconvolution analysis for measuring HEF.

The third example is the application to the quantitative analysis of ^{99m}Tc-diethylenetriamine pentaacetic acid-galactosyl-human serum albumin (GSA) liver scintigraphy.[11] In this study, we developed a simplified method for quantitative analysis of liver scintigraphy with GSA using spectral analysis. Dynamic liver scintigraphy using GSA was performed in three normal volunteers and 19 patients with chronic liver disease. Dynamic data were obtained with a gamma camera for 30 min after the injection of approximately 185 MBq GSA. The rate constant for the liver uptake of GSA from the blood (K_u, min^{-1}), total excretion rate (K_e, min^{-1}) and non-specific volume of distribution (V_h) were obtained by spectral analysis. V_h was defined as the volume in the liver region of interest (ROI) occupied by GSA which was in equilibrium with that in the blood. It should be noted that V_h had no units, since the counts in both the liver and heart ROI were normalized by scan length to obtain counts pixel^{-1} min^{-1}. For comparison, compartment analysis was also performed. A receptor index (LHL_{15}) was calculated by dividing the radioactivity of the liver ROI by that of the liver plus heart ROIs 15 min post-injection. The K_u values obtained by spectral analysis (y) agreed well with those obtained by compartment analysis (x) ($y = 0.953x - 0.013$, r = 0.992, SEE = 0.016 min^{-1}). The K_e and V_h values obtained by spectral analysis (y) correlated significantly with those obtained by compartment analysis (x) ($y = 1.149x - 0.016$, r = 0.826, SEE = 0.017 min^{-1} for K_e; $y = 1.191x + 0.044$, r = 0.975, SEE = 0.021 for V_h). The K_u values obtained by spectral analysis decreased as the severity of liver disease progressed, and were non-linearly related to the LHL_{15} values, suggesting that K_u is more sensitive to liver damage than LHL_{15}, especially in the early stages of liver damage. These results suggest that spectral analysis applied to dynamic liver scintigraphy with GSA provides a simple, non-invasive and useful tool for the quantitative evaluation of liver function. Recently, Sakamoto et al.[12] have applied this method to dynamic SPECT with GSA, and evaluated liver function before and after transarterial embolization (TAE) in a three-dimensional manner.

The fourth example is the application to the renal uptake rate measurement of ^{99m}Tc-dimercaptosuccinic acid (DMSA) using spectral analysis.[13] In this study, we developed a new method for measuring the rate of renal uptake of DMSA using spectral analysis. The renal uptake rate (per minute) of DMSA (K) was calculated by averaging the tissue impulse response function values obtained by spectral analysis between 10 min and 15 min. The K values obtained by spectral analysis correlated well with the renal uptake rates (%) measured 2 h after DMSA administration (r = 0.921 with background correction; r = 0.924 without background correction). There was a good agreement between the K values obtained by spectral analysis using the kidney time-activity curves with (x) and without (y) background correction (r = 0.993, $y = 1.089x + 0.004$), suggesting that our method requires no background correction. There was excellent correlation between the K values obtained by spectral analysis using the kidney time-activity curves with (y) and without (x) kidney depth correction (r = 0.992, $y = 1.721x + 0.000$ with background correction; r = 0.990, $y = 1.720x + 0.000$ without background correction), suggesting that our method requires no kidney depth correction. These results

indicate that spectral analysis is appropriate and useful for the quantification of the renal uptake rate of DMSA. We believe that this method will facilitate even more widespread utilization of the quantitative assessment of DMSA uptake by planar scintigraphy, since it needs only 10–15 min for imaging, and background and kidney depth correction and blood sampling are not required.

The fifth example is the application to dynamic SPECT studies with *N*-isopropyl-*p*-[^{123}I]iodoamphetamine (IMP).[14] This study was performed to evaluate the usefulness of spectral analysis applied to dynamic SPECT studies with IMP. The unidirectional clearance of IMP from the blood to the brain tissue (K_1) obtained by spectral analysis (y, m*l*/g/min) agreed well with that obtained from a two-compartment model using the nonlinear least-squares (NLSQ) method (x, m*l*/g/min) ($y = 0.994x + 0.003$, r = 0.999, SEE = 0.005 m*l*/g/min). The rate constant for back diffusion of IMP from the brain tissue to the blood (k_2) obtained by spectral analysis (y, min^{-1}) also agreed well with that obtained by the NLSQ method (x, min^{-1}) ($y = 0.985x + 0.000$, r = 0.948, SEE = 0.001 min^{-1}). The brain vascular volume (V_0) obtained by spectral analysis (y, m*l*/g) correlated well with that obtained by the NLSQ method (x, m*l*/g) ($y = 1.138x + 0.000$, r = 0.867, SEE = 0.012 m*l*/g). These results indicate that spectral analysis is applicable and useful for quantification of the kinetic parameters of IMP in the human brain, and can be an alternative approach to compartment analysis.

The final example is the application to the estimation of the brain perfusion index for measurement of cerebral blood flow (CBF) using technetium-99m compounds.[15–19] CBF has been quantified non-invasively using the brain perfusion index (BPI) determined from radionuclide angiographic data generated by ^{99m}Tc-hexamethylpropylene amine oxime (HMPAO) or ^{99m}Tc-ethyl cysteinate dimer (ECD). The BPI is generally calculated using graphical analysis. In the present study, BPI was measured using spectral analysis, and its usefulness was evaluated in comparison with graphical analysis. The BPI was calculated from the sum of spectral data obtained by spectral analysis. We applied this method to radionuclide angiographic data collected from the bilateral brain hemispheres of 20 patients with various brain diseases using HMPAO and from those of 20 patients using ECD. We also measured BPI using graphical analysis. The BPI values obtained by spectral analysis (BPI^S) (x) and by graphical analysis (BPI^G) (y) correlated closely ($y = 0.708x + 0.038$, r = 0.945 for HMPAO and $y = 0.559x + 0.093$, r = 0.931 for ECD). However, the BPI^G values were underestimated by 22.9 ± 6.6% (mean ± SD) for HMPAO and by 27.9 ± 7.5% for ECD as compared with the BPI^S values. The extent of underestimation tended to increase with increasing BPI^S values. These findings were considered to be a result of the BPI^G values being affected by the first-pass extraction fraction of the tracer. We also compared the BPI^S and BPI^G values with those of CBF measured using IMP (CBF^{IMP}) in 16 patients (six for HMPAO and ten for ECD). Although both BPI^S and BPI^G values correlated significantly with the CBF^{IMP} values, the correlation coefficient in BPI^S was always better than that in BPI^G (r = 0.869 for HMPAO and r = 0.929 for ECD in BPI^S, r = 0.629 for HMPAO and r = 0.856 for ECD in BPI^G). These results suggest that spectral analysis can provide a more reliable BPI for quantifying CBF using HMPAO or ECD than the conventional method using graphical analysis. Takasawa et al.[17] investigated changes in BPI after the administration of acetazolamide in six healthy male volunteers. They found that according to the BPI^S values, the increase in BPI after the intravenous administration of acetazolamide was 40.1 ± 8.4%, as opposed to an increase of only 11.3 ± 6.5% according to the BPI^G values. These results also suggest that our method will be useful especially when using a tracer with a low first-pass extraction fraction and/or when performing activation studies using pharmacological intervention.

CONCLUSION

In this review, we described the principle and clinical applications of spectral analysis, based on our experience. Spectral analysis can be applied to various dynamic data acquired by planar scintigraphy, SPECT or PET as an alternative approach to compartment analysis. Spectral analysis appears to be clinically useful, because it not only facilitates the interpretation of dynamic scintigraphic, SPECT or PET data, but also simplifies comparisons between regions and between subjects.

ACKNOWLEDGMENT

This study was supported in part by a Grant-in-Aid for Scientific Research (C) (2) No. 13670937 from the Japan Society for the Promotion of Science (JSPS).

REFERENCES

1. Tobler HJ, Engel G. Affinity spectra: a novel way for the evaluation of equilibrium binding experiments. *Naunyn-Schmiedebergs Arch Pharmacol* 1983; 322: 183–192.
2. Cunningham VJ, Jones T. Spectral analysis of dynamic PET studies. *J Cereb Blood Flow Metab* 1993; 13: 15–23.
3. Lawson CL, Hanson RJ. *Solving least squares problems*. Englewood Cliffs, New Jersey; Prentice-Hall, 1974: chapter 23.
4. Phelps ME, Huang SC, Hoffman EJ, Selin C, Sokoloff L, Kuhl DE. Tomographic measurement of local cerebral glucose metabolic rate in humans with (F-18) 2-fluoro-2-deoxy-D-glucose: validation of method. *Ann Neurol* 1979; 6: 371–388.
5. Huang SC, Phelps ME, Hoffman EJ, Siders K, Selin CJ, Kuhl DE. Noninvasive determination of local cerebral metabolic rate of glucose in man. *Am J Physiol* 1980; 238: E69–E82.

6. Kuwabara H, Evans AC, Gjedde A. Michaelis-Menten constraints improved cerebral glucose metabolism and regional lumped constant measurement with [^{18}F]fluorodeoxyglucose. *J Cereb Blood Flow Metab* 1990; 10: 180–189.
7. Murase K, Mochizuki T, Kikuchi T, Ikezoe J. Kinetic parameter estimation from compartment models using a genetic algorithm. *Nucl Med Commun* 1999; 20: 925–932.
8. Murase K, Tsuda T, Mochizuki T, Tanada S, Ikezoe J. Spectral analysis applied to hepatobiliary dynamic scintigraphy with ^{99m}Tc-*N*-pyridoxyl-5-methyltryptophan. *Nucl Med Commun* 1997; 18: 1049–1056.
9. Fukui A, Murase K, Tsuda T, Fujii T, Ikezoe J. Assessment of liver function in chronic liver diseases and regional function of irradiated liver by means of ^{99m}Tc-galactosyl-human serum albumin liver scintigraphy and quantitative spectral analysis. *Ann Nucl Med* 2000; 14: 467–476.
10. Murase K, Tsuda T, Mochizuki T, Ikezoe J. Hepatic extraction fraction of hepatobiliary radiopharmaceuticals measured using spectral analysis. *Nucl Med Commun* 1999; 20: 1041–1045.
11. Murase K, Tsuda T, Mochizuki T, Ikezoe J. A simplified method for the quantitative analysis of ^{99m}Tc-GSA liver scintigraphy using spectral analysis. *Nucl Med Commun* 1998; 19: 219–227.
12. Sakamoto K, Higashino H, Sogabe I, Takahashi Y, Doi M, Yano M, et al. Clinical usefulness of spectral analysis and dynamic SPECT with ^{99m}Tc-diethylenetriamine pentaacetic acid-galactosyl-human-serum albumin (^{99m}Tc-GSA): a quantitative assessment of liver function. The 49th Annual Meeting of the Society of Nuclear Medicine, June 15–19, 2002, Los Angeles, CA, USA (Abstract book, 130p).
13. Murase K, Yamazaki Y, Mochizuki T, Ikezoe J. Renal uptake rate measurement of ^{99m}Tc-dimercaptosuccinic acid using spectral analysis. *Nucl Med Commun* 2002; 23: 265–273.
14. Murase K, Tanada S, Inoue T, Ikezoe J. Spectral analysis applied to dynamic single photon emission computed tomography studies with *N*-isopropyl-*p*-(^{123}I)iodoamphetamine. *Ann Nucl Med* 1998; 12: 109–114.
15. Murase K, Inoue T, Fujioka H, Ishimaru Y, Akamune K, Yamamoto Y, et al. An alternative approach to estimation of the brain perfusion index for measurement of cerebral blood flow using technetium-99m compounds. *Eur J Nucl Med* 1999; 26: 1333–1339.
16. Murase K, Fujioka H, Inoue T, Ishimaru Y, Akamune A, Yamamoto Y, et al. Reproducibility of the brain perfusion index for measuring cerebral blood flow using technetium-99m compounds. *Eur J Nucl Med* 2001; 28: 1640–1646.
17. Takasawa M, Murase K, Oku N, Yoshikawa T, Osaki Y, Imaizumi M, et al. Assessment of acetazolamide reactivity in cerebral blood flow using spectral analysis and technetium-99m hexamethylpropylene amine oxime. *J Cereb Blood Flow Metab* 2002; 22: 1004–1009.
18. Takasawa M, Murase K, Oku N, Kawamata M, Imaizumi M, Yoshikawa T, et al. Automatic determination of brain perfusion index for measurement of cerebral blood flow using spectral analysis and ^{99m}Tc-HMPAO. *Eur J Nucl Med* 2002; 29: 1443–1446.
19. Takasawa M, Murase K, Oku N, Kawamata M, Nagayoshi M, Osaki Y, et al. Interobserver variability of cerebral blood flow measurements obtained using spectral analysis and technetium-99m labeled compounds. *Ann Nucl Med* 2003; 17: 255–259.